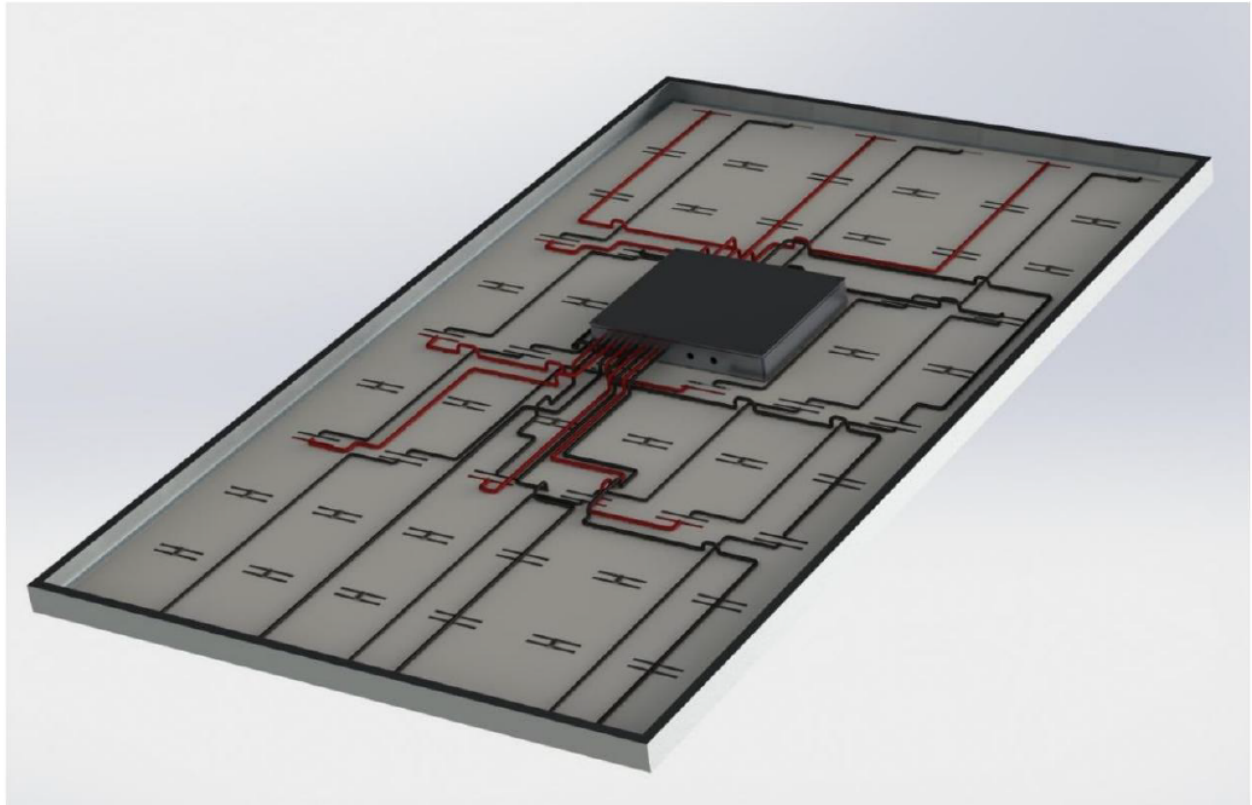


Customized Smart Mismatch-Tolerant Module CSMTM



Final report (confidential)

Project details

Projectnumber: TEUE 1721102
Project title: Customized Smart Mismatch-Tolerant Module
Coordinator: Universiteit Utrecht
Partners: Heliox, Kameleon Solar
Project period: 1 February 2018 – 31 December 2021

Contact details

This report is created by the project partners: Utrecht University, Heliox, Kameleon Solar. For questions regarding the project, results and follow-up projects you can contact:

Universiteit Utrecht

Wilfried van Sark, Sara Golroodbari

+31 30 2537611

w.g.j.h.m.vansark@uu.nl, s.z.mirbagherigolroodbari@uu.nl

Subsidy

The project was supported with a subsidy from the Dutch Ministry of Economic Affairs, National EZ subsidies, Topsector Energie, performed by the Rijksdienst voor Ondernemend Nederland (RVO).

Acknowledgements

We would like to explicitly like to thank the following students from the Utrecht University of Applied Sciences (Hogeschool Utrecht) in assistance in designing a new on-board electronics system: Marnix Remming, Niels van der Zijden, Silas Witmond, and Teun Drijfhout, as well as their teacher at HU Joost Kouijzer.

Cover

The picture on the cover © HU.

Summary

Varying irradiation conditions across photovoltaic (PV) modules may lead to nonlinear power losses due to the interconnection topology of solar cells within modules. This mismatch may lead to highly localized power dissipation (hotspots), and local heating which can cause irreversible damage to the module.

This project aimed 1) to develop a smart module that considerably mitigates mismatch effects, including partial shading and temperature differences for different cells, 2) to perform hot spot detection and design hotspot protection, 3) to design and develop integrated electronic circuitry for the smart module, and 4) to perform financial analysis for large-scale manufacturing.

A smart module was developed that is mismatch resilient, and which is equipped with a multi-objective algorithm to both maximize the harvested energy and fulfil DC bus requirements. Hot spot phenomena have been investigated infrared (IR) thermography and a novel hot spot detection method has been developed. Dedicated design electronic circuits have been developed including a bill of materials and cost analysis. However, due to Covid and the unavailability of many electronic components, hardware realisation was not possible.

Preface

This final report describes the work performed in the project CSMTM (Customized Smart Mismatch-Tolerant Module) as carried out within the framework of the Nationale regelingen EZ-subsidies, Topsector Energie, executed by the Rijksdienst voor Ondernemend Nederland. The report addresses the results obtained. In addition, several project changes, mostly due to the Covid pandemic, are described.

Contents

Summary.....	3
Preface.....	4
Contents	5
1. Introduction	6
2. Goal and purpose.....	8
3. Results.....	10
3.1. Modelling.....	10
3.2. Hot spot detection method and testing.....	13
3.2. IR thermography.....	17
3.2. Active hotspot protection method	19
3.3. Prototyping new design	26
3.4. Financial aspects	31
4. Discussion	33
5. Follow up activities	34
6. Dissemination	35
References	36
Appendix.....	38

1. Introduction

Energy harvesting in PV systems is made possible via maximum power point tracking (MPPT) of the current-voltage (I-V) curve implemented in an (micro)inverter and generally works fine. However, partial shading (dormer windows, chimneys, poles, bird droppings, soiling) causes a mismatch between modules of a system and between cells of a module. Besides MPPT per module in the system, dynamic reconfigurations (DR) [1]–[4] have also been suggested to enhance shade resilience. The nonlinear effect of mismatch conditions (MC), e.g., partial shading conditions (PS), either decreases the efficiency and accuracy of the MPPT algorithms or makes the tracking time longer [5]–[8]. In DR methods which are implemented at the module level, the configuration within PV modules is to change between one topology for cell interconnection to another, in a dynamical manner. These methods may be very complicated regarding their optimization algorithm and perform noticeably slow [9]–[11]. Another way to mitigate the PS effects on the performance of a PV system is to divide the module into several groups of PV cells, as we have proposed earlier [1]. This smart module architecture comprises a buck DC-DC converter for each group of cells which performs as an optimizer for that group of cells. In this architecture, each group of cells consists of a number of cells connected in series (see Figure 1).

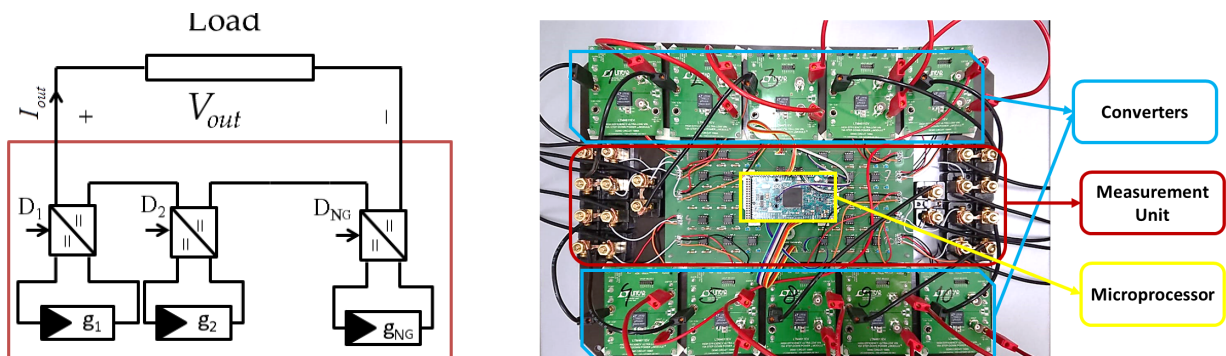


Figure 1.- Design of groups of cells in the smart module and electronics design [1].

module power [12], or in the case of the smart module, reduces the group power. Usually, bypass diodes are implemented to mitigate hot spotting; however, they do not prevent hot spots from occurring nor limit the potential damage they may cause. An active hot spot detection technique should be used to find the hot spot area. Furthermore, the smart module requires an electronics circuit to be mounted at the back of the panel, which generates heat during operation, and this may change the temperature of adjacent cells, which may decrease the group power, as it causes temperature differences (TD) and as a

consequence voltage differences within the group. To solve this problem, we suggest two solutions: 1) to reduce the size of the electronic circuit in order to reduce heat generation, and 2) to control the TD effect in the module. It should be noted that the TD effect may occur for other reasons than heat generated by the electronic circuit at the back of the panel.

Challenge

To mitigate the effect of TD on the cells which causes output voltage and eventually output power decrease, we need to solve a multi-objective optimization problem which maximizes the output power from each group of cells by controlling both voltage and current of the group of cells and at the same time the resulting voltage and current should comply with input specifications of the inverter that is connected to the module.

Photovoltaic (PV) hot spotting is a temporary fault condition that occurs in series-connected PV cells and modules. To mitigate this issue, an active hot spot detection method should be developed. Here we propose to use I-V curve recording from each group of cells. The method can be validated by means of infrared (IR) thermography.

The microinverters and electronics circuits in the present smart module need a redesign, taking into account the following aspects:

- (i) Due to the fact that electronic elements may generate heat, it is preferable for each chip to include more than one converter. Therefore, the customized integrated circuit (IC) may generate less heat and needs less space. This change will also decrease the price of the smart module.
- (ii) The customized chip should be equipped with a control system, to make the algorithm much simpler for the main microprocessor. Therefore, a simpler microprocessor may be used in the final circuit.
- (iii) Incorporation of the hot spot protection method.

2. Goal and purpose

Questions to be answered

As the philosophy behind designing the smart, shade-resilient module is to harvest the maximum energy from the cells at low levelized cost of energy (LCoE), the important issues in smart module design can be found in the answer to the following questions:

- How can the lifetime of the module be prolonged?
- How can the module cheaper be made cheaper?

This requires answering the following sub-questions:

1. How to control the micro converters considering the effects of both PS and TD, by defining a multi-objective optimization problem?
2. What is the location/cell at which a hot spot occurred?
This needs a hot spot detection method which can detect this phenomenon in real time.
3. How can one mitigate the hot spot causes with hot spot protection via variation in the control signal for the converter or minor changes in the electrical circuit?
4. How can one design a customized chip for micro converters and make the electronic circuit cheaper and smaller in size?

Scope and goal of the project

This project's scope is to perform scientific research on a smart PV module to maximize the harvested energy at different mismatch conditions which have effects on PV output power. The module is also equipped with an active hot spot protection method.

The goal of the project is to create a smart module and prolong its lifetime to be ready for mass production and the market.

Results of the Project

The results of the project are:

1. Model of a redesigned smart module considering TD effects.
2. IR thermography technique analysis
3. Hotspot detection method.
4. New hardware designs.
5. Integrated circuit design and development.
6. Building the hardware of the smart module equipped with the mentioned methods.

Use of the result in the market

This project develops, tests and delivers a robust mismatch resilient smart module that can be used for residential and industrial PV systems which are potentially prone to shading or TD.

The hotspot detection method can readily be implemented in the smart module and protect the module from damage after the failure is detected. As a result, the module lifetime will be prolonged.

Furthermore, temperature effect control and customized chip design can both boost up the harvested energy from the panel. This all will lead to better cost efficiency.

It is important to mention that the market for this product is not limited to the Netherlands but also in many other countries where PV deployment in the built environment is targeted. Also, the results can be directly used in building integrated PV (BIPV) components and interconnections.

The Technology Readiness Level (TRL) of the present smart module design is TRL4. The proposed redesign has aspects of TRL1 and TRL2. Using the present smart module the final product will have reached TRL5, with a clear outlook on how to further develop the product to TRL 7 and higher.

3. Results

3.1. Modelling

A model for the complete smart module considering the groups designed before has been modified allowing to include temperature difference effects between different cells. The temperature variation in this model is a function of both ambient temperature and heat arising from electronics elements. Measured data are implemented in the model and a comparison between the developed smart module and a standard series-connected module available in the market is made.

For modeling the smart module, we consider the surface of the 60-cell module to consist of 600,000 (600k) pixels, which means that each solar cell has 10 kpixels (ignoring inter-cell distances for simplicity). The

irradiation level on pixel p is called G_p and is given in $G_p = \begin{cases} G_{p,GHI} & \text{if it is not shaded} \\ G_{p,s} & \text{if it is shaded} \end{cases}$

Equation 1:

$$G_p = \begin{cases} G_{p,GHI} & \text{if it is not shaded} \\ G_{p,s} & \text{if it is shaded} \end{cases} \quad \text{Equation 1}$$

where $G_{p,GHI}$ is the global horizontal irradiance (GHI) at the pixel and $G_{p,s}$ the irradiance at the pixel under the shaded condition.

To calculate the irradiation level on each cell Equation 2 is used, which is based on experimental results from a study by Sinapis et al. [12]:

$$G_c = (F_{unshaded} \times G_{GHI}) + (F_{shaded} \times G_{dif}) \quad \text{Equation 2}$$

where $F_{unshaded}$ is the unshaded fraction of cell, F_{shaded} is the shaded fraction of cell, G_{GHI} is the global horizontal irradiance, G_{dif} is the diffuse irradiance at the cell C. The most shaded cell in each group N_i determines the output current of that group.

The performance of the smart PV module needs to be tested under realistic shading conditions. In this study two different shading conditions are considered: (1) Random shadow, which might result from the effect of dust, bird droppings, snow, etc.; and (2) pole shadow, which is caused by a static obstacle during daylight, and which is mostly caused by pole shapes, chimneys, dormers, or a part of the building on the roof. Also, these shading conditions can be combined [13].

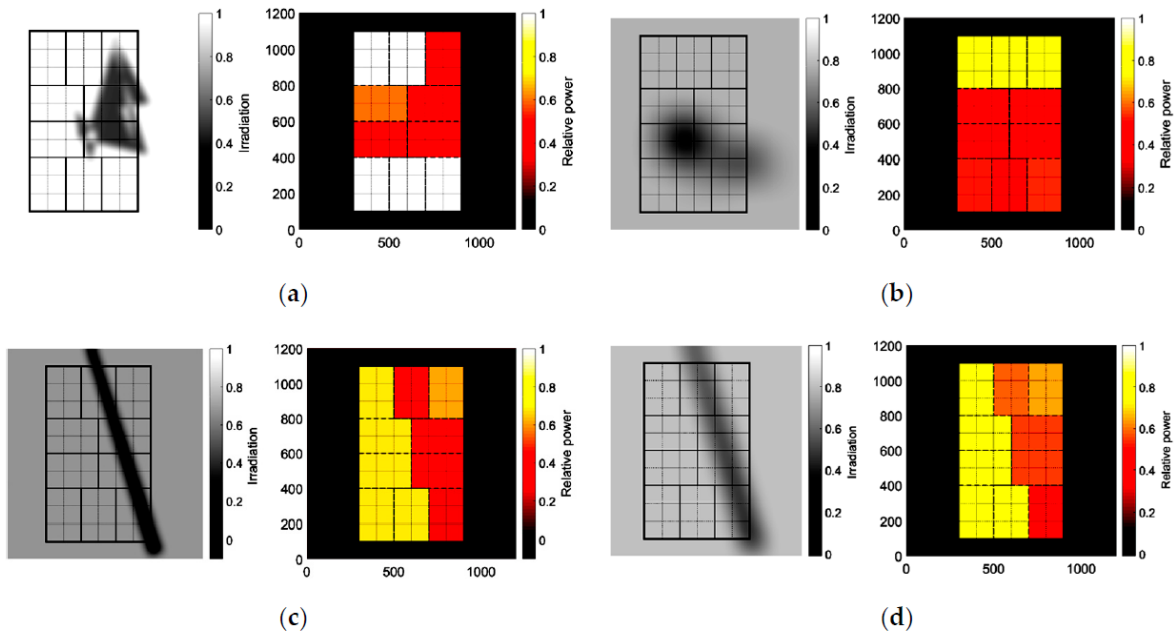


Figure 2. Examples of shading pattern, (a) Random shading for higher diffuse to direct irradiation, (b) Random shading for lower diffuse to direct irradiation, (c) Pole shading for higher diffuse to direct irradiation, (d) Pole shading for lower diffuse to direct irradiation [13]

Figure 3 shows recorded irradiance data during the experiments. Three different time frames of 15 min in duration are used for shading experiments. Figure 4, 5 and 6 show different shading patterns and their effect on groups of PV cells for different architectures. Unlike in Figure 5 and Figure 6, which only have the effect of pole shadow, in Figure 4 a combination of both pole and random shadows is shown. The output power for three time frames as shown in these figures is given in Table 1. It is clearly shown that a series connected architecture in time frame 1 performs very weak, as a result of the bypass diodes in this architecture. The shade pattern in time frame 1 affects both current and voltage significantly. The group of cells under much darker shadow are bypassed by BPDs and current is very low because of the shading. Each time frame simulates 15 min of the real world with the assumption of having a constant value of irradiation variables.

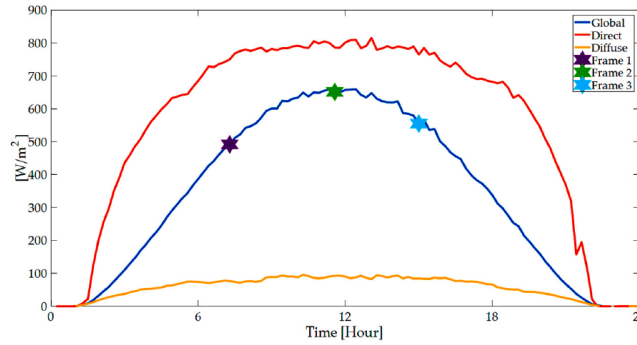


Figure 3 Global, Direct and Diffuse irradiation levels during the experiments.

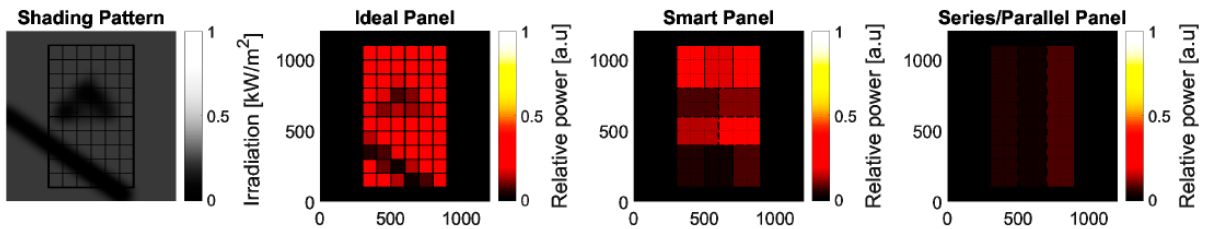


Figure 4. Combined pole and random shading patterns and effect of that on different architectures at time frame 1.

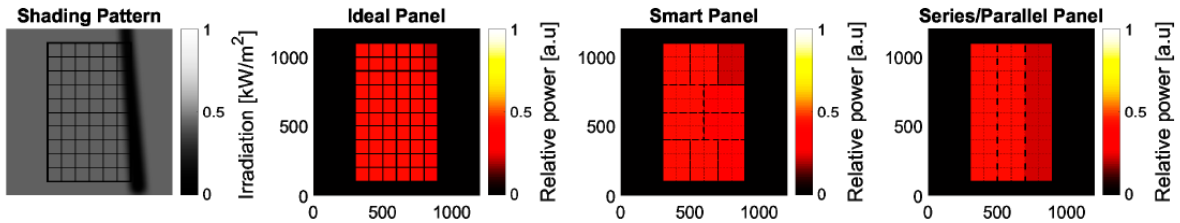


Figure 5. Pole shading pattern and effect of that on different architectures at time frame 2.

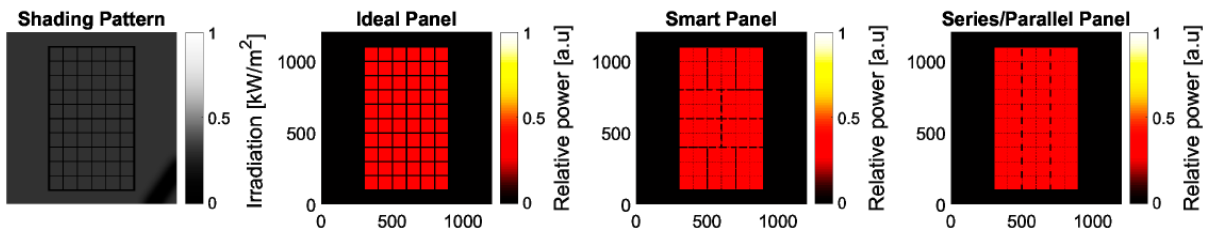


Figure 6. Pole shading pattern and effect of that on different architectures at time frame 3.
Note that the shade is not cast on the panel.

Table 1 Output power in the three time-frames indicated in Figure 3..

Architecture	Frame (1)	Frame(2)	Frame(3)
Ideal Architecture	48.35 (W)	84.23(W)	116.54(W)
Smart Architecture	18.49 (W)	69(W)	108.85(W)
Series Connected Architecture	0.84(W)	30.95(W)	112.35(W)
Parallel Connected Architecture	4.51(W)	62.97(W)	113.42(W)

3.2. Hot spot detection method and testing

Experimental results have shown that when a PV cell string is under a maximum power point tracking control, hot spotting in a single cell results in a capacitance increase and DC impedance increase. This may be used to detect the hot spot in real time by implementing appropriate tools to measure both I-V curve and capacitance in the cells. This is implemented in an adapted version of the model developed in section 3.1, so as to investigate the occurrence of hot spot phenomena. The results from this model are used later to be compared with IR analysis.

For having a fair comparison, the module is divided into two sections, a smart and a conventional section. In the smart section, we connected each group of cells to one buck converter and connect all converters in series to their output side.

Different shading patterns are applied to the testing. Furthermore, a test run is conducted without any shading, shown in Figure 7. To be able to compare the results of both halves of the module it is imperative that both halves receive the same shading pattern. This rules out the possibility of using natural fouling sources during the tests, because this would result in a random and most likely different pattern for both halves [14]. At the start of testing each pattern the panel is cleaned to minimize the effect of natural fouling build-up.

The following shading patterns are tested during this research:

1. A pole shadow. As shown in Figure 8, an identical pole is placed vertically in front of each half of the panel to ensure that both halves of the panel are shaded in the same manner. To this end a PVC tube with a diameter of 750 mm is used.
2. A heterogeneous non-transparent pattern to represent the effect of bird droppings, moss growth etc. This pattern is applied directly to the surface of the panel and made equal for both halves of the panel. To achieve this, shapes are cut out of cardboard and placed at the top of the panel, demonstrated in Figure 9.
3. A homogeneous semi-transparent pattern. A mosquito curtain is placed across the entire panel to simulate the effects of homogeneous fouling such as dust and pollen, displayed in Figure 10.



Figure 7: No shade testing setup.



Figure 8: Pole shadow testing setup.



Figure 9: Bird drop testing setup.



Figure 10: Homogenous fouling testing setup.

The smart module applies MPPT at a sub module level, where six cells are grouped and connected in parallel to a DC-DC converter. The groups of cells are then connected in series to form the module. This smart module implements a sweep method MPPT algorithm per group of cells and has been simulated, prototyped and practically tested on a short time frame [13,15]. The results showed a significant increase in the output power under PS conditions, compared to a conventional panel.

The prototype testing described before was performed on the timeframe of one hour, while almost half of the panel were covered by shade and the rest was shaded by a pole shaped and some dynamic obstacles. To better assess the benefits and potential downsides of this smart module topology longer outdoor testing is therefore required. The smart module also has the potential to decrease the occurrence of hotspots due to smaller cell grouping [16].

The measured irradiance in the plane of the module and the temperature of the module throughout the testing day are shown in Figure 11. Some intermittent cloud coverage occurred during the testing day which results in the fluctuations in irradiance. Furthermore, the temperature of the module also changed throughout the day. These changing conditions make the data and results not suitable for direct comparison between different test conditions. However, the data recorded from both halves during each test can be compared since both halves were operating at the same conditions at that time.

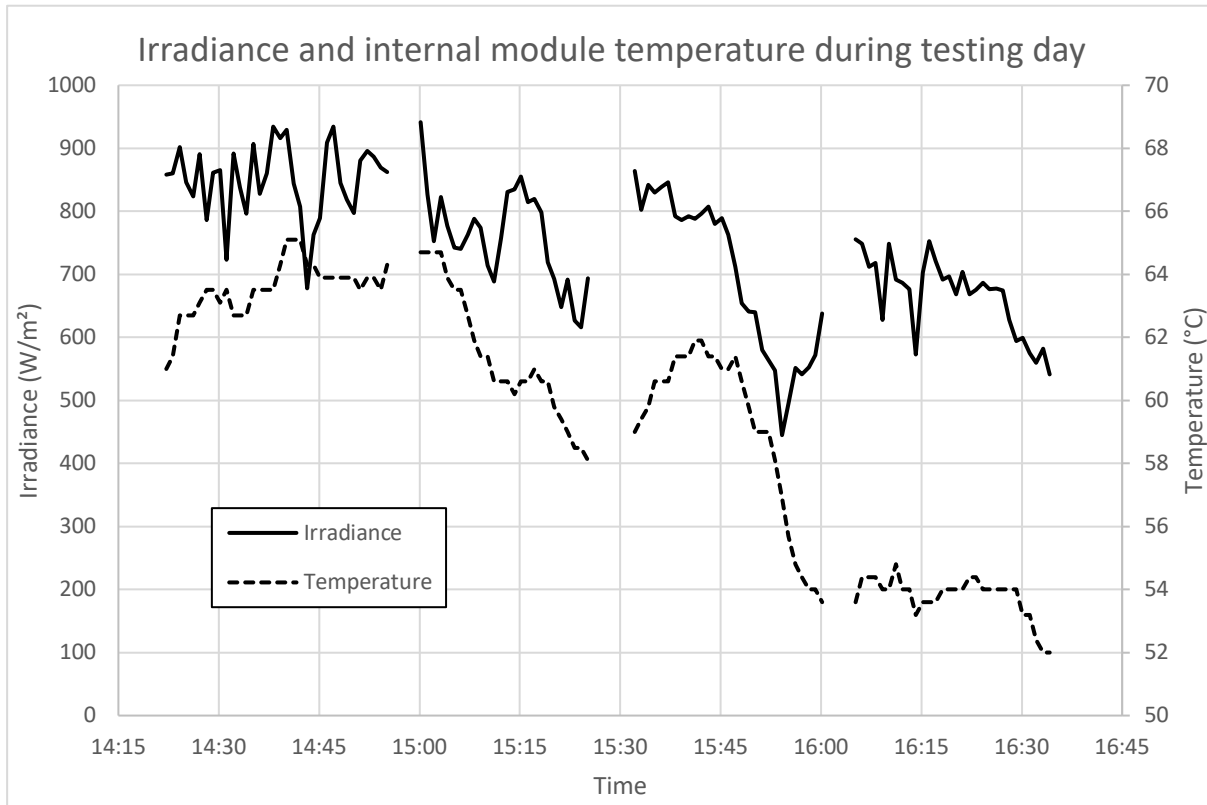


Figure 11: Irradiance during testing day.

During analysis it is found that group one due to breakage in the circuit did not function correctly during the tests. These different characteristics result in a lower power output of this group as can be seen in Table 2. Hence, group one is removed from the results and only groups two to five are taken into consideration.

Furthermore, it is found during the latter two tests, namely the bird drop and homogenous shade tests, the efficiency of group five which is read from the measuring part, is significantly higher than the other groups of the smart half. Further analysis shows that this higher efficiency is the result of a higher

Table 2: Average efficiency of the module areas during the tests.

	G1	G2	G3	G4	G5	Smart	Conventional	Relative
No shade	3.4%	5.7%	6.3%	4.6%	5.8%	5.6%	5.2%	108%
Pole shade	4.6%	6.9%	8.3%	6.0%	6.7%	7.0%	5.3%	131%
Bird drop	5.7%	8.0%	7.5%	7.2%	11.3%	7.6%	5.8%	132%
Homogenous fouling	4.2%	5.3%	7.0%	7.0%	10.1%	6.4%	4.4%	146%

measured voltage, while the current is similar to the other groups. Such a difference in efficiency is expected to result in a difference in temperature of the cells. However, this is not the case. Thus, most likely the difference is the result of a measurement error while in reality the group operates similarly to the other groups, which is proved by using a multimeter. A likely explanation for this error could be that the voltage divider, which is used for measuring the voltage output, is not functioning linearly anymore that might be due to the damage to the voltage divider's resistors. This combined with the changing irradiance and temperature throughout the tests results in an inaccurate voltage measurement during the latter two tests. This difference in output voltage is not noticeable in the first two tests. Most likely because the operating conditions were still close enough to the conditions under calibration. Therefore, the efficiency of group five during the latter two tests is excluded from the average efficiency of the smart half. Nevertheless, the results in terms of hotspot development can still be considered relevant since the group was operating nominally.

The average efficiency of each group within the smart half, the average efficiency of the smart half and conventional half during the tests are presented in Table 2. Counterintuitively, the efficiency of both halves is not highest during the test without shade present. For the smart half the efficiency is even at its lowest during the test without shade present. However, the output power was highest during this test as can be seen in Table 3. Note that in this table the column of the smart half only contains the sum of the included groups, which is corrected for size. A cause for the higher efficiency during the PS and fouling tests is that the average irradiance was highest during the test without shade present. The testing module has a relatively high internal resistance due to extra wiring. The increase in current due to the higher irradiance combined with the high internal resistance causes the module to operate less efficiently. Furthermore, the module temperature was at the highest level during the test without shade present, which also causes a decrease in efficiency.

Table 3: Average power output of the modules areas during the tests in watts.

	G1	G2	G3	G4	G5	Smart	Conventional
No shade	4.6	7.7	8.5	6.3	7.8	38.0	35.2
Pole shade	5.6	8.5	10.2	7.3	8.2	42.7	32.6
Bird drop	6.1	8.7	8.1	7.8	12.2	41.0	31.1
Homogenous fouling	4.6	5.7	7.6	7.6	11.0	34.9	23.9

The exclusion of groups one and five result in a relatively larger shaded area for the smart half compared to the conventional half during the pole shadow and bird drop tests. Filtering for this difference in shaded area is not feasible due to the non-linear response of PV-systems to partial shading. However, even under a larger relative shade the smart half is more efficient during all tests (see column “relative” in Table 2).

3.2. IR thermography

Two light source set-ups have been constructed in order to perform IR thermography, one based on a series of construction (halogen) lamps (Figure 14), and a LED setup (Figure 12). In the LED setup, 26 LED strips with each 512 LEDs per meter and five meter per strip were glued to an aluminium panel of 1m×1.6m×0.0015m. The aluminium panel in combination with the aluminium structure worked as a heat exchanger to get rid of the excess heat from all the lights. Total intensity of all LEDs together was 130,000 lumen. The aluminium was folded on the sides to ensure as much light as possible reaching the panel. The panel was placed at a distance of about 20 centimetres away from the lights in an aluminium frame. For every image that was made with the IR camera, the hinges were temporarily unscrewed, and the picture was made while the panel would be slightly tilted. For the smart setup the same smart board was connected with the PV panel as for the setup with construction lights. The same holds for the in series setup. Additionally, the LED setup was tested in a different room which was roughly a third of the size of the room used for the construction light setup.

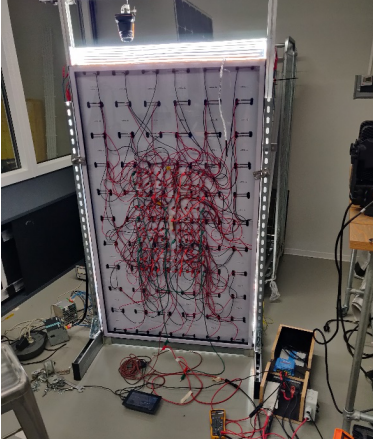


Figure 12. LED test setup wired in series.



Figure 13. Example of the object for creation of shadow on the PV panel. In the figure it is hanging on against the panel during one of the test rounds

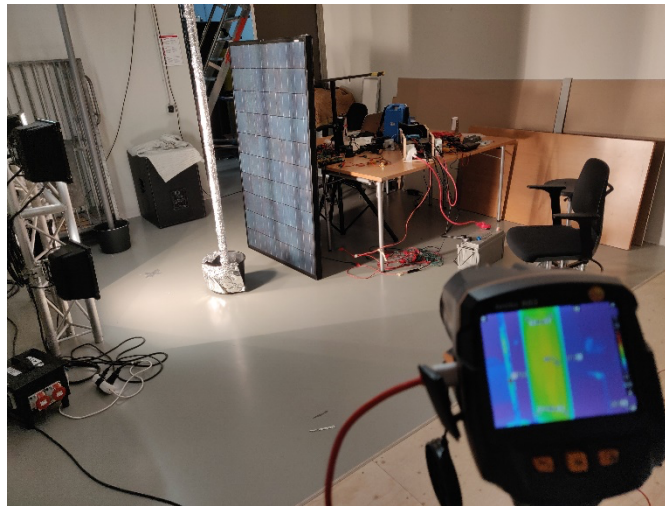


Figure 14. Point-of-view of the IR camera for making images for first four test rounds.

For the creation of a shadow, a plastic package was wrapped in aluminium foil which could shade one cell. It was attached to wire that was wrapped in aluminium foil as well. In this way the object could be moved over the panel hanging from the top of the panel. The object can be seen in Figure 13.

An infrared (IR) camera was placed in front of the panel. An example from the construction lights setup can be seen in Figure 14. The thermal imaging camera that was used is the Testo 883 [17]. This camera was able to make an IR image simultaneously with a normal photo and was able to measure the temperature with a precision of 0.1 K. Therefore, it was possible to analyse the thermal images in detail afterwards. This camera was adjusted in height in such a way that no shadow was created on the modules and no light reflection was seen.

3.2. Active hotspot protection method

An active hotspot protection method is proposed that uses an electrical circuit along with the micro converters in the smart module to bypass the group of cells where the hotspot occurs. Once a group of cell performs as load instead of current source, which can be detected by measuring the group current and voltage continuously, active BPDs will be used that perform like soft switches in case of hotspot detection. Cells under the hotspot condition will be bypassed with the corresponding active BPD.

A very accurate optimization method should be implemented for grouping the number of cells per active BPD. Because once the hot spot is detected, all cells in the same group will be bypassed.

Several tests have been done for this part of research. However due to similarity in the results, we only present some of the images.

Indoor laboratory testing

First, indoor tests have been performed, with either halogen or LED lamps as light source. For Tests 1.1 and 1.2 halogen lamps are used as source of light, and for Tests 2.1 and 2.2 the LED source described before has been used.

Test 1.1: pole shading

As shown in Figure 15 a test has been done with pole shading. It can be seen that the panel is cooler in the shaded part except in the middle of the shade. However, looking at the normal image it can be seen that the positioning of the lamps leads to two shades from the pole as it is placed near the panel. This explains the hotter part. Also, below on the images a small red dot is seen. However, looking closely at the normal image it can be seen that this spot is not the panel, but results from the bucket in which the pole is placed.. Furthermore, the differences in temperature within the shaded parts can reach up to 15 °C and the temperature difference of the non-shaded parts can be up to 20 °C higher compared to the shaded parts.

Test 1.2: pole shading

Figure 16 shows no points with much higher temperatures within the shaded areas. The shaded areas have a lower temperature than the non-shaded parts with a difference of up to 15 °C. The differences within the shaded parts reach up to 10 °C. Also, the images show that two shades are created due to the positioning of the construction lamps.

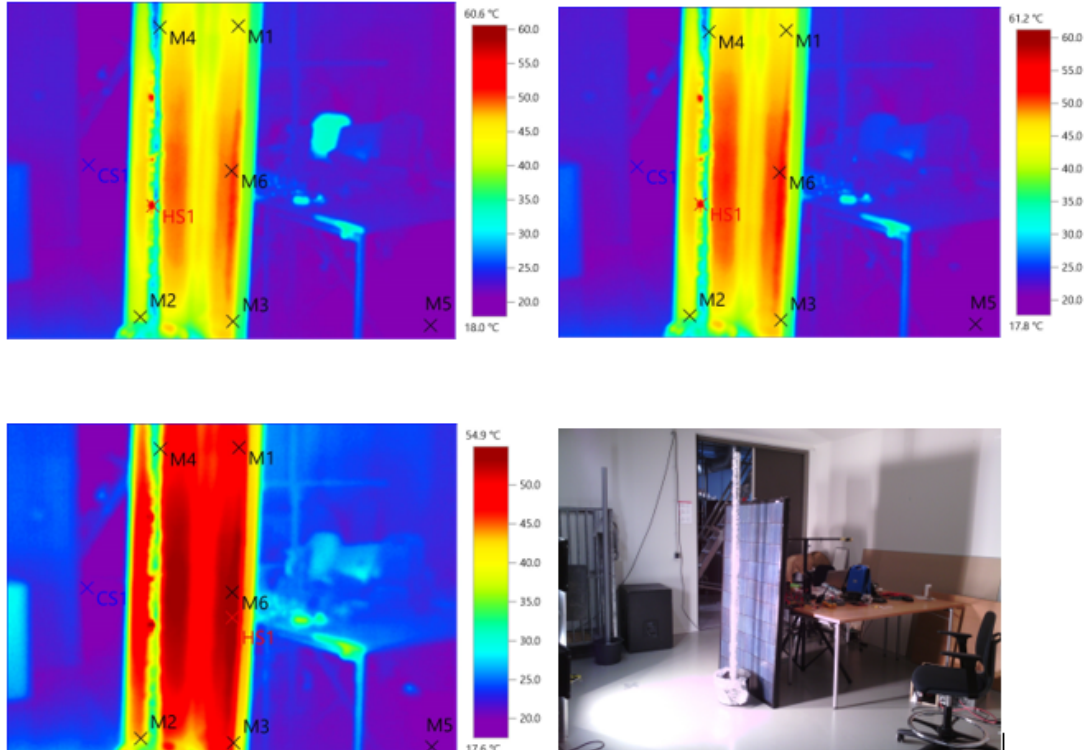


Figure 15 Overview of Test 1.1: showing three IR images and one normal image. Note: legends next to images are different

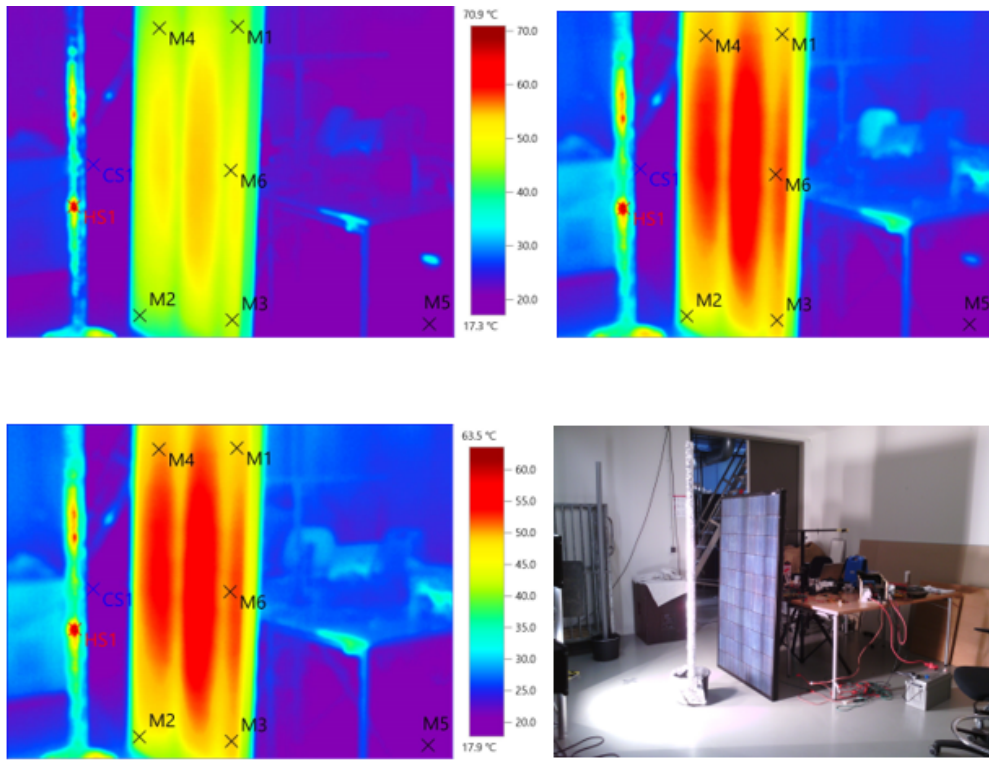


Figure 16 Overview of Test 1.2: showing three IR images and one normal image. Note: legends next to images are different.

Test 2.1: smaller obstacle shading

In

Figure 17, no hotspots are seen in the shaded parts when the object is removed for analysis of the shaded parts. In the images on the left a large hot area is seen with a higher temperature than its surrounding. But, looking at the images on the right the hot area moves when the object is moved. Furthermore, the shaded parts can differ up to 5 °C with its surroundings and the temperature of these parts can be up to 10 °C lower than the non-shaded parts.

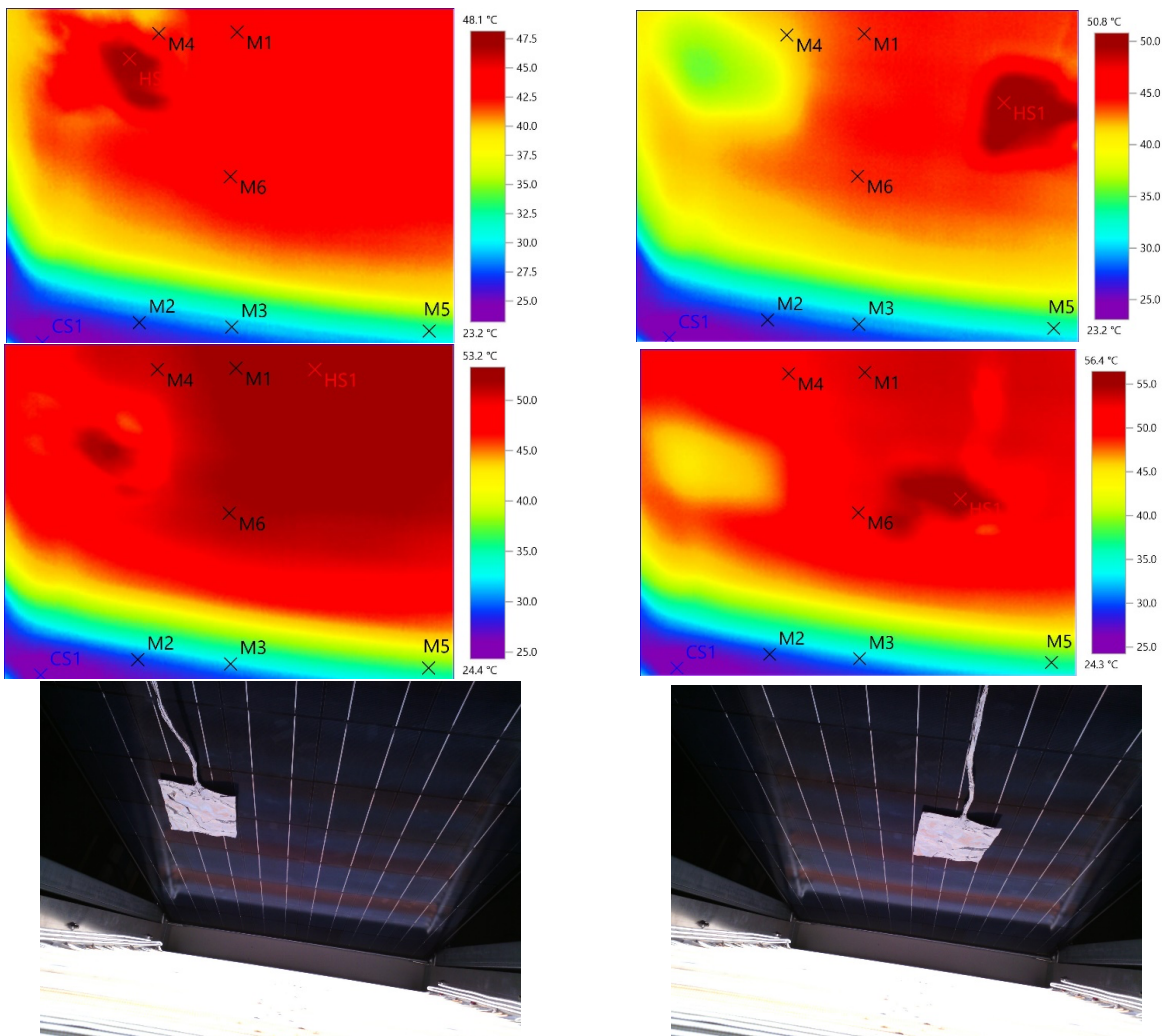


Figure 17. Overview of Test 2.1 showing two moments checked for hotspots. In the images on the left the object is in place and on the right the object is moved to the right. The last two images show the normal images. Note: legends next to images are different.

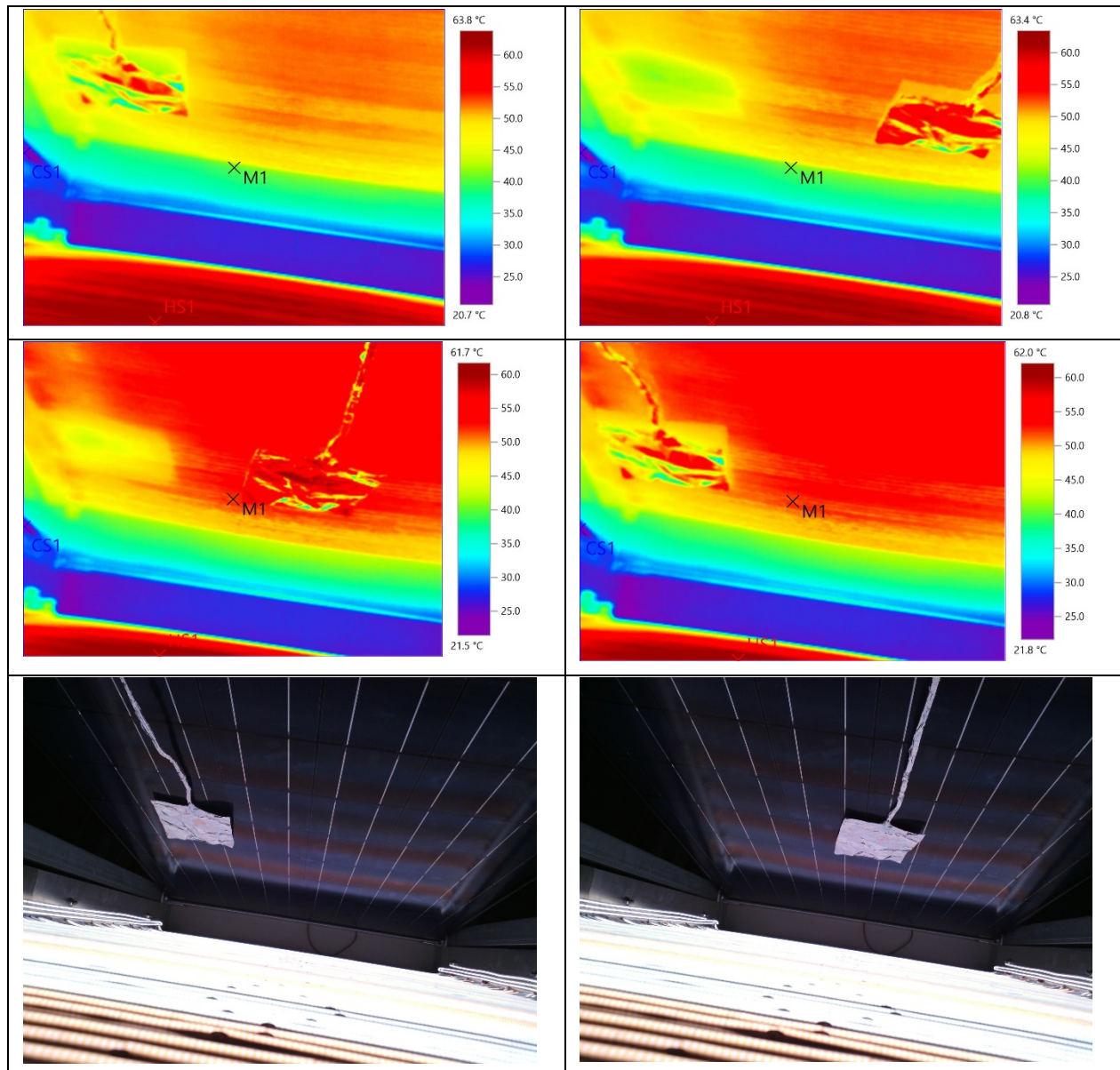


Figure 18. Overview of Test 2.2: showing two moments checked for hotspots. In the images on the left the object is in place and on the right the object is moved to the right. The last two images show the normal images. Note: legends next to images are different

Test 2.2: smaller obstacle shading

In the two moments checked for hotspots from shading in

Figure 18 no spots with higher temperatures are seen compared to their surroundings. The shaded area was always colder than its direct surroundings. Only at the lower end of the panel a lower temperature is measured. However, from the normal images it can be seen that less light reaches this area. On the contrary, it cannot be seen whether the temperatures measured are only the panel itself or also the heat

reflection of the LED lights. Furthermore, the temperature differences within the shaded areas reach up to 5 °C and the non-shade parts are 10 to 15 °C lower than most of the panel. Only the lower end of the panel is colder. Also, hot and cold spots are seen in the images with a much higher temperature than its surroundings. However, comparing these images with the normal images it can be seen that these are heat reflections from the object.

Outdoor testing with natural light

An image of the test setup during the four tests is already shown in Figure 7 to Figure 10. The cells of the module are grouped as shown in Figure 19. The infra-red (IR) images taken during all tests are presented in Figures 20-27. These figures include an image taken at the start and end of the test. The temperature colour scale shown next to Figure 19 is the same for all other IR images (Figure 20-27).

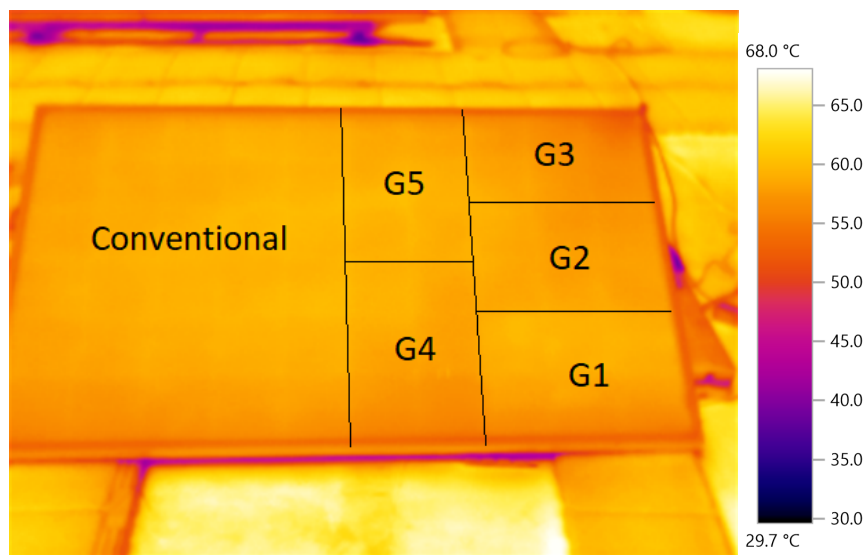


Figure 19. Division of the cells into groups

The lower efficiency of group 1 results in the observation that the cells of this group are slightly warmer than the surrounding cells. Measurement points M1 and M2 in Figure 21 have respective temperatures of 58.2 and 56.9 °C, thus a temperature difference of 1.3 °C.

During the bird drop test (Figure 24, 25) a hotspot developed in the third cell from the left in the topmost row of cells (Group 5). On the smart half this same shading pattern did not result in a hotspot forming. In Figure 25 measurement point M1 is placed on the hotspot and M2 is placed on the same

location on the smart half. The respective temperature of these measurement points are 53.1 and 49.0°C, thus a temperature difference of 4.1°C. No hotspots developed during any of the other tests.

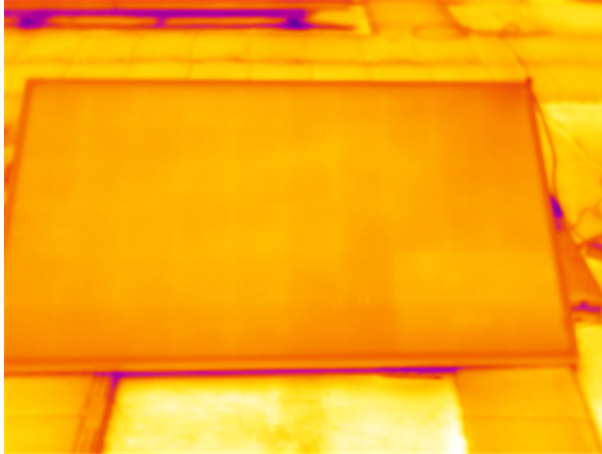


Figure 20: IR image at beginning of no shade test

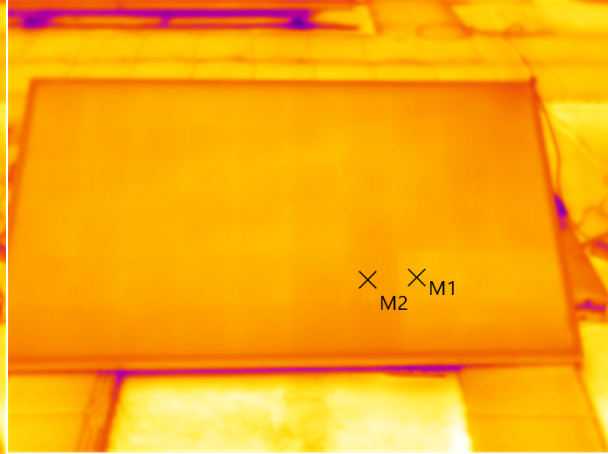


Figure 21: IR image at end of no shade test

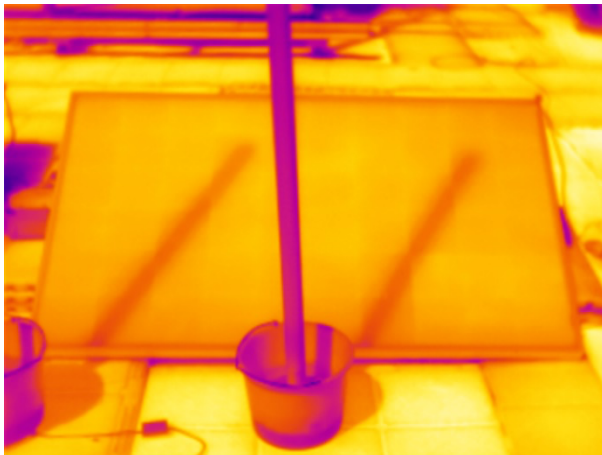


Figure 22: IR image at beginning of pole shadow test

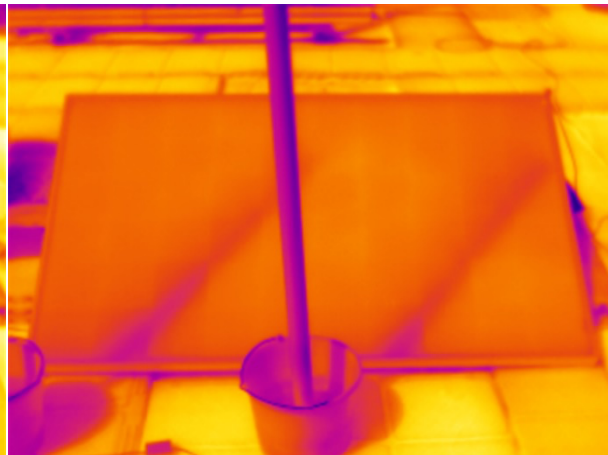


Figure 23: IR image at end of pole shadow test

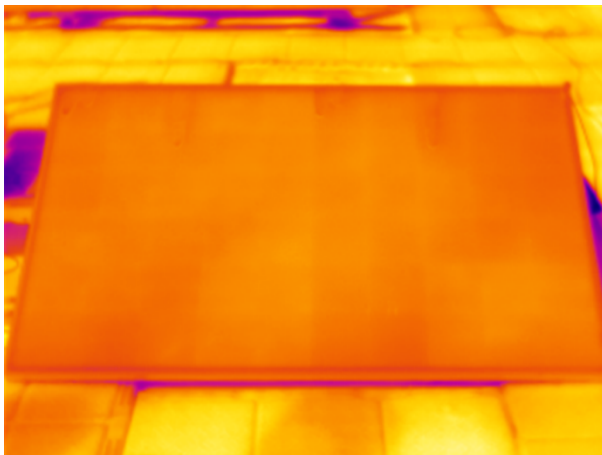


Figure 24: IR image at beginning of bird drop test

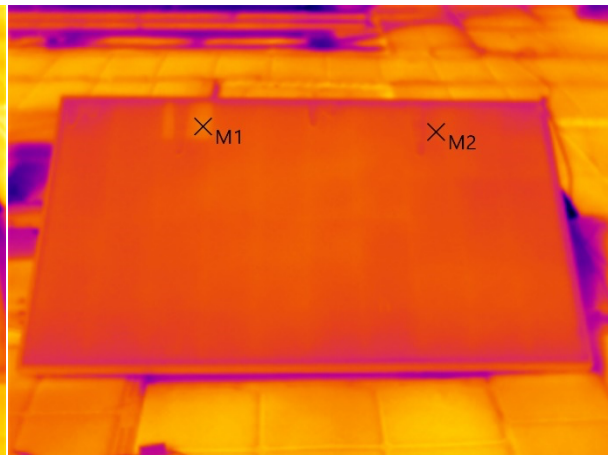


Figure 25: IR image at end of bird drop test

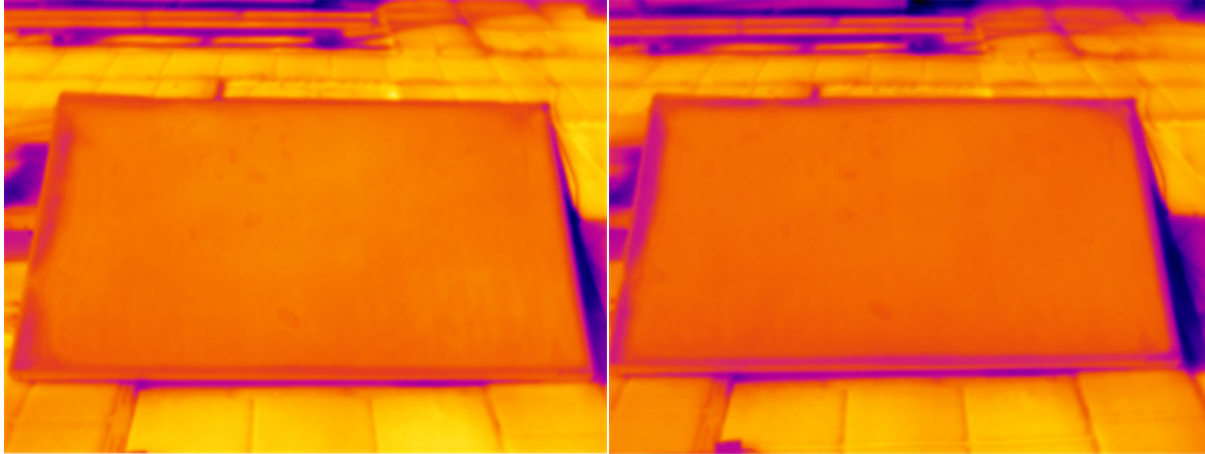


Figure 26: IR image at beginning of homogeneous shade test Figure 27: IR image at end of homogeneous shade test

3.3. Prototyping new design

Based on the results on the new hot spot protection method, the electrical circuit needs to be redesigned for the improved smart module.

The present prototype has a lot of long cables and conventional electronics elements. To avoid extra losses based on that, it is better to change the electronics designs. First, we need to change all elements to so-called surface mount device (SMD) elements to decrease the losses and make the assembly procedure easier.

In the new design we considered the following functions to be added/edited to/from the old design based on our experimental testing:

- 1- Current sensing: this can be done with either of the following options to prevent resistive losses
 - a. Hall effect sensor: This sensor can measure the current through a cable by measuring the amplitude of the magnetic field surrounding the cable through the Hall effect. This sensor therefore does not have to be placed in the circuit itself but can be placed in close proximity. This prevents losses that normally occur in any chip due to internal resistance in the silicon and bond wires. The measurements do depend on a circuit that does not radiate excess electromagnetic interference (EMI) from components or wires whose current is not to be measured.
 - b. microchip: for measuring currents, microchips have been developed by several manufacturers that only perform this task. The reading of the data with the current values is done by means of a communication protocol performed. Common examples of this are

I2C and SM-Bus, standard protocols that many modern microcontrollers support. All logic is contained in one component, which keeps communication between them consistent and at high efficiency.

- 2- Voltage sensing: instead of the voltage divider, which is used in old design, the circuit can be modified using:
 - a. ADC (analog to digital converter): The maximum voltage that the ADC will see is = 3.67 V, a voltage that most ADCs can easily handle these days. By selecting an ADC that has a maximum conversion voltage just above that point, the greatest amount of dynamic range can be utilized. This has the advantage that fewer components are involved, which prevents losses and keeps overall tolerance higher.
 - b. microchip: as mentioned for current sensing there are chips available that can only perform this task extremely well. Chips are also available that merge the current and voltage measurements into a single chip, simplifying the scheme even more. These types of chips can therefore be read by means of commonly used communication protocols such as I2C and SM-Bus. Examples of this are several chips from the Texas Instruments INA series. These chips are very accurate, fast and simple to use.
- 3- Export data: In order for any users and/or technicians to see the collected data from the solar panel, appropriate data export must be added. This can be done either wirelessly or via a wired connection to the solar panel.
- 4- Keep water out: this can be done using O-ring or Cork/metal gasket.
- 5- Keep EMI out, it could be done implementing Metallic tape, aluminium housing or a metallic mesh around the box. A common way to reduce the effects of EMI is to make smart use of the PCB on which the electronics must already be mounted. There are many different ways to limit emissions by placing a lot of copper in smart places on the printed circuit board (PCB). The first way to do this is to use a smart stack-up. A stack-up is a method where different layers of a PCB are used for specific purposes. A stack-up that is widely used because it is simple and works well is a 4-layer stack-up. The advantage of this is that components on the top and bottom have a small path to ground, which reduces noise.
- 6- Heat dissipation, for heat dissipation we considered a heat sink which covers the box and underneath the box, there should be layer of isolation to prevent the heat flux direction going toward the back sheet.

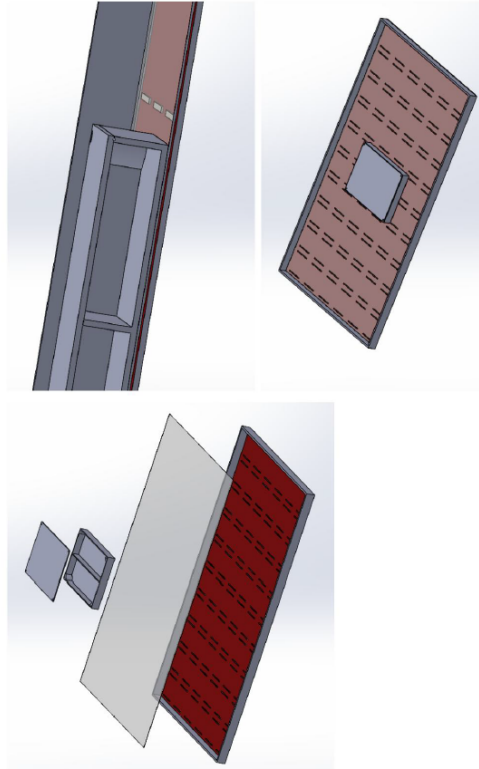


Figure 28. 3D model of the central box

For the new electronics design we considered two different options:

- (i) **Scattered converters**, a separate box is made for each group of cells, which contains the sensor and buck converter. This idea is not the best idea due to the housings, cables and shielding which have to be made ten times and is very costly, and this makes the system more vulnerable to errors, and difficult to repair.
- (ii) **Central box**. Instead of putting all sensors and converters in their own box, all electronics are put in one box housing, the concept is shown in Figure 28. A potential disadvantage compared to the first idea is that the microprocessor is in the same housing. This needs extra consideration regarding its shielding. It can also be an advantage, because the distance from the sensors to the processor is smaller. Dissipating heat in this way is a bit more difficult as all electronics and associated heat production are in one place.

A number of simulations were performed to determine the material to be used for the housing. For these simulations, a thermal study in Solidworks was used. There are many options for the material, but the most common options are: plastic and aluminum. For the simulation, 1060 aluminum and ABS plastic were used.

To run a thermal analysis simulation, a 35-watt heat source is placed in the housing of the electronics which consists of all electronics devices in the housing. The back sheet temperature is assumed to be 50°C.

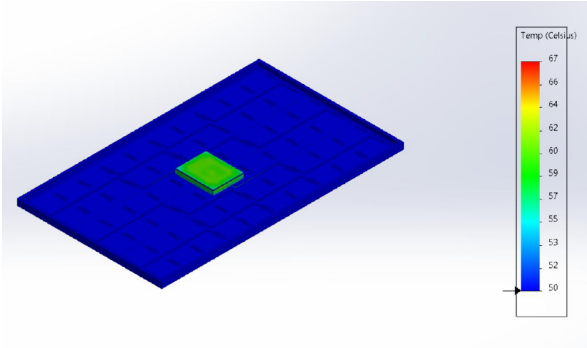


Figure 29 Simulation results for ABS

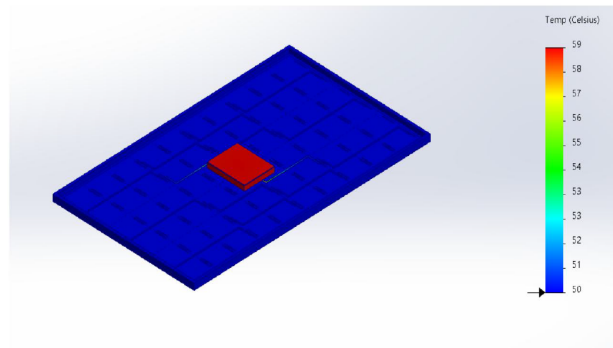


Figure 30 Simulation results for aluminum

From the simulation results shown in Figures 29 and 30 it can be concluded that the inside surface of the ABS housing is around 70°C while the aluminum housing only reaches 60 °C.

A new PCB has been designed in collaboration with Hogeschool Utrecht (HU), such that all elements are located in one PCB. To this end, SMD components need to be used to allocate less space and bring circuits of converter, and controller all in one PCB.

The schematic drawing of the PCB is shown in Figure 31 and is divided into 11 different parts to maintain a good overview. Left and right to the middle **STM32F103C8T6** microcontroller are ten identical groups that consist of a **LTM4611EV** buck converter that requires an **INA226** to measure the voltage and current, an **MCP4151** to adjust to change the set output voltage, and an **AD626ANZ** to generate a differential voltage for the **INA226** voltage measurements. Renderings of the back of the actual panel are shown in Figure 32 and 33.

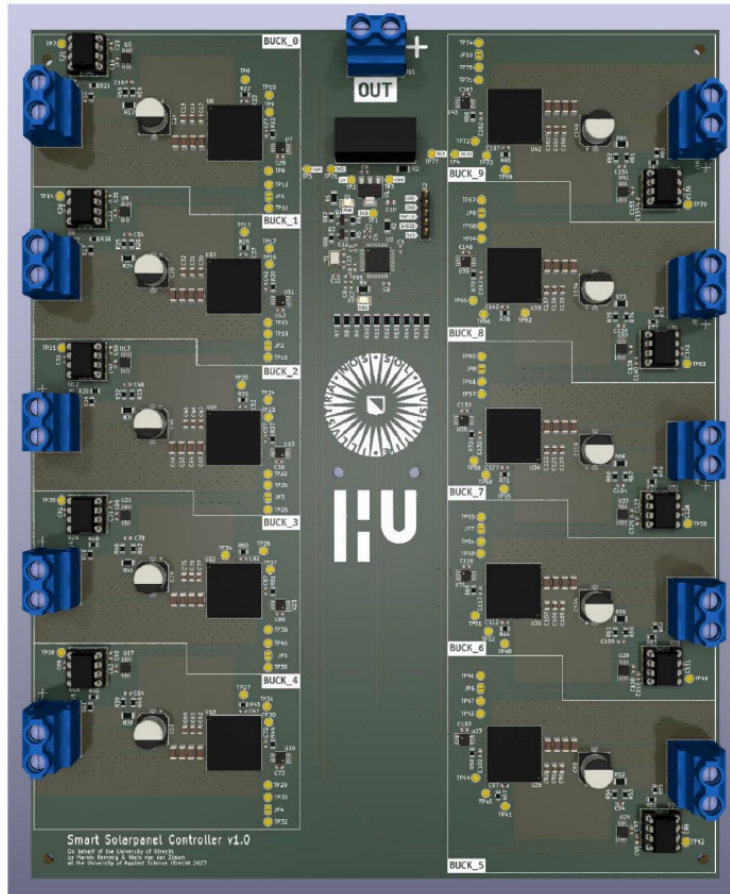


Figure 31. Computer representation of the final version of the PCB.

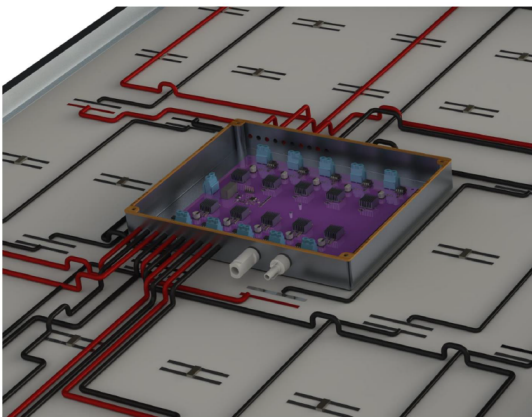


Figure 32. Back of the panel with the housing without a cover

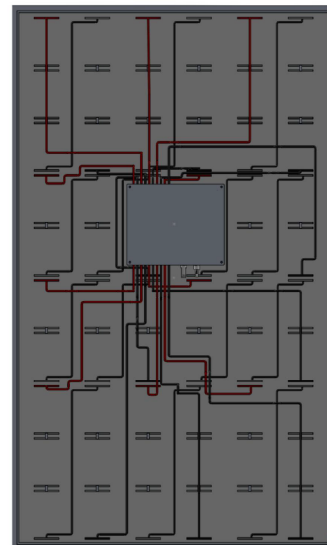


Figure 33. Cabling on the back of the panel

Due to the chip and electronics element shortage in the past years, the hardware preparation of this new design could not be completed.

3.4. Financial aspects

The bill of materials (BOM) for all mechanical and electronics needed for one smart module are shown in Table 4. However, it should be taken into consideration that the prices are based on purchasing small amounts which makes the final total cost quite expensive. Moreover, the chip price at the time of this project is increased due to IC shortage which started from the year 2021. The most important cost is related to the LTM4611EV buck converter, about 65% of total cost. Alternatives in the market must be found. Assuming a present standard module cost of 0.2 €/Wp [18], and a module of 420 Wp, module cost would be 84 €. For a smart module to be competitive on the market, the present cost calculated from the bill of materials, should be lowered by at least a factor of 50. This is realistic only if large volumes of smart modules are manufactured.

Table 4: Bill of materials for the smart module and costs.

Element	Condition	Amount	price/item (€)	Total price (€)
Nickel strip	10 mm wide	1000 mm lang	2.99	2.99
Black solar panel cable	6mm ²	13 meter	1.40	18.20
Red solar panel cable	6mm ²	5 meter	1.40	7
Aluminium plate 3 mm	540 x 280	1	35.41	35.41
Aluminium round 12 mm	150 mm	1	1.05	1.05
M6 x 30 Phillips head bolt		4	5	5
MC4 connectors	1 male, 1 female	2	1.045	2.09
Silicone sealant		1 tube	2	2
Rubber plate 2 mm	1x 240	290 mm	5	5
CL10B104KA8NNNC	100nF	46	0.024	1.104
CL10B105KP8NNNC	1uF	12	0.036	0.42
CL10A106MQ8NNNC	10uF	2	0.1	0.2
0603N120J500CT	14pF	2	0.09	0.18
EMK0JM331FB0D00R	330uF	10	0.195	1.95
CL21A226MQQNNNE	22uF	31	0.088	2.728
CL10A475KQ8NNNC	10nF	10	0.037	0.37
GRM31CD80J107MEA8K	100uF	40	0.32	12.8
06031U101FAT2A	100pF	10	0.225	2.25
LTST-C230KGKT	PWR_LED	1	0.29	0.29
LTST-C230KGKT	DGB_LED	1	0.29	0.29
2506031217Y2	120R	1	0.09	0.09
TB005-762-02BE	1 x 2 Scr.Term	11	0.56	6.182
Transistor_FET:BS170FTA	BS170	2	0.66	1.32
RMCF1206FT1K50	1k5	2	0.032	0.064
ERJ-8ENF2672V	26k7	1	0.18	0.18

RMCF1206FT10K0	10k	1	0.032	0.032
RC0805FR-131K5L	1k5	4	0.031	0.124
RMCF0805FT100K	100k	10	0.024	0.24
PA1206FRE472U5Z	OR0025	10	0.497	4.97
ESR10EZPF10R0	10R	20	0.16	3.2
RT0805BRE079KL	9k	10	0.307	3.07
RMCF0805FT1K00	1k	10	0.069	0.69
RMCF0805FT10K0	10k	10	0.06	0.69
ERA-6AEB203V	20k	10	0.031	0.31
AZ1117IH-3.3TRG1	AZ1117-3.3	1	0.38	3.8
Isolated Buck	17791069215	1	13.7	13.7
STM32F103C8T6	STM32F103C8T6	1	6.28	6.28
AD626ANZ:AD626ANZ	AD656ANZ	10	0.341	3.41
Analog_ADC: INA226	INA226	10	3.09	30.9
LTM4611EV	LTM4611EV-PBF	10	31.15	311.5
MCP4151	MCP4151-02E/SN	10	1.14	11.4
TSX-3225 16.0000MF20X-W6	16MHz	1	0.4	0.4
				482

4. Discussion

CSMTM was an ambitious project with innovative and challenging objectives given the available budget. It was even more challenging when the Covid pandemic hit the world. This hampered experimental work due to restrictions, but also led to increased prices for many electronic components. As a result, the project was quite delayed, and the actual realisation of new hardware was not possible.

The consortium regrets that the project has not led to the maximum success for which the project was set up. On the other hand, we are confident that our smart module design is able to address shading issues very well. Commercial success will depend on large-scale manufacturing, and we see an opportunity in initiative to bring PV production back to Europe, focusing on technologies that we in Europe are good at, which includes shade resilient BIPV modules.

5. Follow up activities

The CSMTM project has resulted in a proof-of-concept of a smart shade-resilient module and an electronics design that is much smaller in size than the original prototype design. Together with Hogeschool Utrecht we will investigate how to realize an actual smart module, which will be tested at UU's testing facility for modules. Based on business model canvas approaches, an assessment will be made for a potential start-up with HU students to develop this smart module electronics design.

6. Dissemination

Dissemination activities have aimed to promote non-confidential results obtained within the project as swiftly and effectively as possible for the benefit of the whole (scientific) community and to avoid duplication of R&D efforts. In particular, smart module experimental results have been shared with experts of the IEA-PVPS Task 13 (“Reliability and Performance of Photovoltaic Systems”) group, and some of these are part of the following report:

M. Littwin, F. Baumgartner, M. Green, W. van Sark, Performance of New Photovoltaic System Designs, IEA-PVPS, Report number IEA-PVPS T13-15: 2021, April 2021, ISBN: 978-3-907281-04-8. (https://iea-pvps.org/wp-content/uploads/2021/03/IEA-PVPS_Task-13_R15-Performance-of-New-PV-system-designs-report.pdf)

Published papers

S.Z. Mirbagheri Golroodbari, A.C. de Waal, W.G.J.H.M. van Sark, *Proof of concept for a novel and smart shade resilient photovoltaic module*, IET-Renewable Power Generation, vol. 13, pp. 2184-2194, 2019.

Conference contributions

Sara Mirbagheri Golroodbari, Wilfried G.J.H.M. Van Sark, *Implementing Smart Panels to Mitigate Mismatch Conditions for a Dynamic Off-shore Floating PV System*, 8th World Conference on Photovoltaic Energy Conversion (WCPEC-8), Milano, Italy 26-30 September 2022 (poster)

Student reports

Boyd Beerling, Hotspot testing of a shade resilient smart photovoltaic panel, M.Sc. Thesis Energy Science, 2022.

Marnix Remming, Niels van der Zijden, Silas Witmond, Teun Drijfhout, Smart Module Design, B.Sc. Quest Project HU, 2022.

PR of project and further PR possibilities

The project partners would like to be approached for any further publicity activities and would like to contribute to public activities of the Rijksdienst voor Ondernemend Nederland or the TKI-Urban Energy and are happy to add these insights to the debate about the energy transition in the Netherlands.

References

- [1] S. M. Golroodbari, A. de Waal, and W. van Sark, "Improvement of Shade Resilience in Photovoltaic Modules Using Buck Converters in a Smart Module Architecture," *Energies*, vol. 11, no. 1, p. 250, Jan. 2018.
- [2] V. Salas, E. Olias, A. Barrado, and A. Lazaro, "Review of the maximum power point tracking algorithms for stand-alone photovoltaic systems," *Sol. energy Mater. Sol. cells*, vol. 90, no. 11, pp. 1555–1578, 2006.
- [3] A. Bidram, A. Davoudi, and R. S. Balog, "Control and Circuit Techniques to Mitigate Partial Shading Effects in Photovoltaic Arrays," *IEEE J. Photovoltaics*, vol. 2, no. 4, pp. 532–546, Oct. 2012.
- [4] C. Olalla, D. Clement, M. Rodriguez, and D. Maksimovic, "Architectures and Control of Submodule Integrated DC–DC Converters for Photovoltaic Applications," *IEEE Trans. Power Electron.*, vol. 28, no. 6, pp. 2980–2997, Jun. 2013.
- [5] S. Z. Mirbagheri, M. Aldeen, and S. Saha, "A PSO-based MPPT re-initialised by incremental conductance method for a standalone PV system," in *Control and Automation (MED), 2015 23th Mediterranean Conference on*, 2015, pp. 298–303.
- [6] A. Reza Reisi, M. Hassan Moradi, and S. Jamasb, "Classification and comparison of maximum power point tracking techniques for photovoltaic system: A review," *Renew. Sustain. Energy Rev.*, vol. 19, no. 0, pp. 433–443, 2013.
- [7] S. M. Mirhassani, S. Z. M. Golroodbari, S. M. M. Golroodbari, and S. Mekhilef, "An improved particle swarm optimization based maximum power point tracking strategy with variable sampling time," *Int. J. Electr. Power Energy Syst.*, vol. 64, pp. 761–770, 2015.
- [8] R. B. A. Koad, A. F. Zobaa, and A. El-Shahat, "A Novel MPPT Algorithm Based on Particle Swarm Optimization for Photovoltaic Systems," *IEEE Trans. Sustain. Energy*, vol. 8, no. 2, pp. 468–476, Apr. 2017.
- [9] S. Serna-Garcés, J. Bastidas-Rodríguez, and C. Ramos-Paja, "Reconfiguration of Urban Photovoltaic Arrays Using Commercial Devices," *Energies*, vol. 9, no. 1, p. 2, Dec. 2015.
- [10] G. Velasco-Quesada, F. Guinjoan-Gispert, R. Pique-Lopez, M. Roman-Lumbreras, and A. Conesa-Roca, "Electrical PV Array Reconfiguration Strategy for Energy Extraction Improvement in Grid-Connected PV Systems," *IEEE Trans. Ind. Electron.*, vol. 56, no. 11, pp. 4319–4331, 2009.
- [11] D. Nguyen and B. Lehman, "An Adaptive Solar Photovoltaic Array Using Model-Based Reconfiguration Algorithm," *IEEE Trans. Ind. Electron.*, vol. 55, no. 7, pp. 2644–2654, 2008.
- [12] K. Sinapis, C. Tzikas, G. Litjens, M. van den Donker, W. Folkerts, W.G.J.H.M. van Sark, A. Smets, "A comprehensive study on partial shading response of c-Si modules and yield modeling of string inverter and module level power electronics," *Solar Energy*. vol. 135, pp. 731-741, 2016.
- [13] S.Z. Mirbagheri Golroodbari, A.C. de Waal, W.G.J.H.M. van Sark, "Improvement of Shade

- Resilience in Photovoltaic Modules using Buck Converters in a Smart Module Architecture," *Energies*, vol. 11, pp. 250, 2018.
- [14] N. Hussain, N. Shahzad, T. Yousaf, A. Waqas, A.H. Javed, S. Khan, M. Ali, R. Liaquat, "Designing of homemade soiling station to explore soiling loss effects on PV modules," *Solar Energy*, vol. 225, pp. 624-633, 2021.
- [15] S.Z. Mirbagheri Golroodbari, A.C. de Waal, W.G.J.H.M. van Sark, "Proof of concept for a novel and smart shade resilient photovoltaic module," *IET-Renewable Power Generation*, vol. 13, pp. 2184-2194, 2019.
- [16]. R.C.N. Pilawa-Podgurski, D. J. Perreault, "Submodule integrated distributed maximum power point tracking for solar photovoltaic applications," *IEEE Transactions on Power Electronics*, vol. 28, pp. 2957-2967, 2012.
- [17] <https://www.testo.com/en-US/testo-883/p/0560-8830>
- [18] Fraunhofer ISE, Photovoltaics Report 2022
<https://www.ise.fraunhofer.de/en/publications/studies/photovoltaics-report.html>

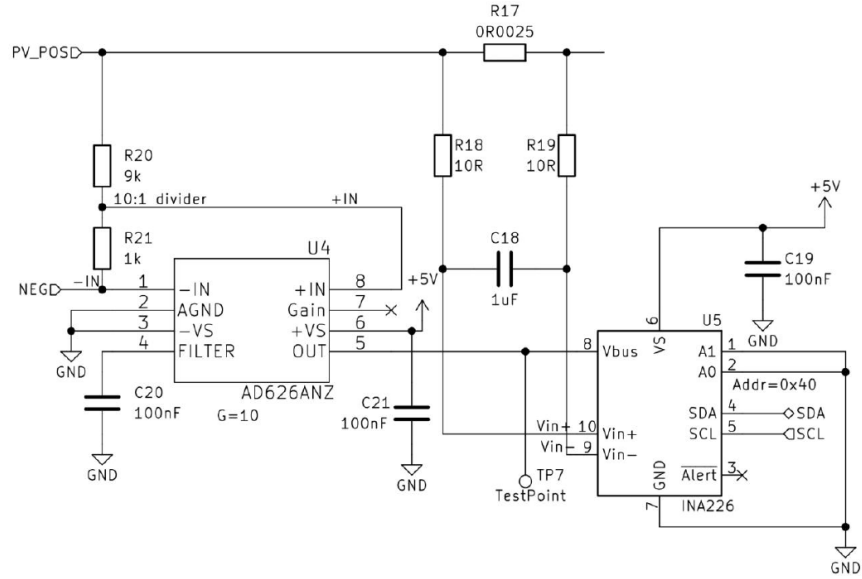


Figure A2. Technical drawing INA226

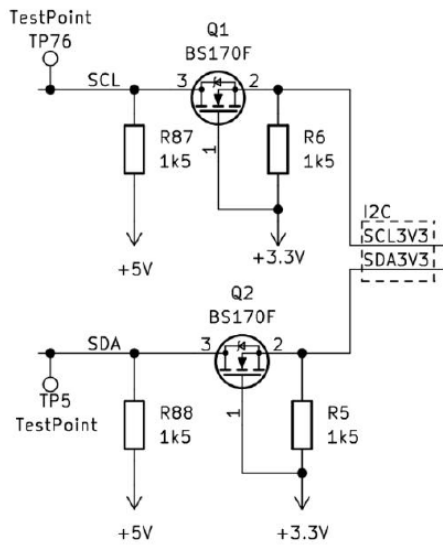


Figure A3. Schematic drawing AD626ANZ

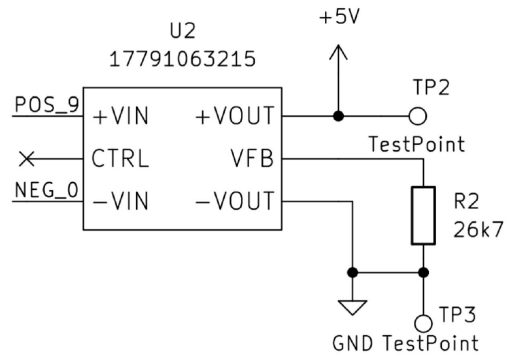


Figure A4. Schematic drawing 17791063215 Buck converter